Investigation of the effect of the doping order in GaN nanowire p-n junctions grown by molecularbeam epitaxy

Omar Saket, Junkang Wang, Nuno Amador-Mendez, Martina Morassi, Arup Kunti, Fabien Bayle, Stéphane Collin, Arnaud Jollivet, Andrey Babichev, Tanbir Sodhi, et al.

Investigation of the effect of the doping order in GaN nanowire p-n junctions grown by molecular-beam epitaxy

Omar Saket[1], Junkang Wang[1], Nuno Amador-Mendez[1], Martina Morassi[1], Arup Kunti[1], Fabien Bayle[1], Stéphane Collin[1], Arnaud Jollivet[1], Andrey Babichev[2], Tanbir Sodhi[1], Jean-Christophe Harmand[1], François H. Julien[1], Noelle Gogneau[1] and Maria Tchernycheva[1*]

[1] Centre de Nanosciences et de Nanotechnologies (C2N), UMR 9001 CNRS, Université Paris Saclay, 91120 Palaiseau, France
[2] ITMO University, 197101 St. Petersburg, Russia

E-mail: maria.tchernycheva@c2n.upsaclay.fr

Received xxxxxx
Accepted for publication xxxxxx
Published xxxxxx

Abstract

We analyse the electrical and optical propreties of single GaN nanowire p-n junctions grown by plasma-assisted molecular-beam epitaxy using magnesium and silicon as doping sources. Different junction architectures having either a n-base or a p-base structure are compared using optical and electrical analyses. Electron-beam induced current microscopy of the nanowires shows that in the case of a n-base p-n junction the parasitic radial growth enhanced by the Mg doping leads to a mixed axial-radial behavior with strong wire-to-wire fluctuations of the junction position and shape. By reverting the doping order p-base p-n junctions with a purely axial well-defined structure and a low wire-to-wire dispersion are achieved. The good optical quality of the top n nanowire segment grown on a p-doped stem is preserved. A hole concentration in the p-doped segment exceeding 10^{18} cm^{-3} was extracted from electron beam induced current mapping and photoluminescence analyses. This high concentration is reached without degrading the nanowire morphology.

Keywords: nanowires, GaN, doping, EBIC, PAMBE

1. Introduction

The discovery of the p-type doping of nitride semiconductors using Magnesium (Mg) impurities in 1989 [1–3] enabled novel optoelectronic applications, the main one being the developement of energy saving solid state lighting [4]. However, reaching high hole concentration in nitrides is challenging due to the limited solubility of Mg in GaN, to the high activation energy of the Mg acceptor and to compensation problems [5–7]. The nanowire (NW) geometry is favorable for nitride p-doping thanks to a decreased formation energy of defects at the surface [8] and to the possibility to relax the compressive strain induced by Mg incorporation [9, 10]. In addition, the small NW footprint is also favorable for achieving dislocation-free growth on a variety of lattice-mismatched substrates like Si [11] or non-conventional substrates [12, 13], which is particularly important for device applications. A large number of studies has been dedicated to the plasma-assisted molecular-beam epitaxy (PAMBE) growth of Mg-doped GaN NWs [14–19]. It

was shown that Mg doping incorporation may be inhomogeneous over the NW volume with a tendency to segregate at the NW lateral surfaces [20, 21]. Nevertheless, the NW morphology was confirmed to be favorable for Mg incorporation and a high hole concentration was reported not only in GaN NWs [22, 23] but also in a more challenging case of Al-rich AlGaN alloys [18, 24–28].

Due to the NW nanoscale diameter, doping quantification in NWs is not straightforward. Hall measurements are indeed extremely challenging in NWs [29–31]. The most popular way to estimate the NW doping concentration is based on contact-free optical methods, namely luminescence or Raman spectroscopy [32–38]. However optical methods require a separate calibration, for example using photoelectrochemical measurements [23]. Scanning probe microscopy can also be used to assess doping: e.g. Kelvin probe force microscopy and the electron beam induced current microscopy (EBIC) were successfully applied to assess carrier concentrations in GaN NW p-n junctions [22, 39].

It was reported by different groups, that high Mg doping is accompanied with a morphological degradation of the NWs, promoting in particular a shell formation [22, 23]. Apart from a few exceptions [40, 41], most of the axial junction nitride NW devices use a p-n or a p-i-n junction with the p-segment grown on top [42–45]. The parasitic p-doped shell formed during the top segment growth may be an issue for these devices since it changes the current injection / extraction path [46] and also makes difficult the doping quantification using electrical methods. Reverting the doping order can solve these problems. Memory effects are known to be reduced in the MBE growth of nitrides compared to the Metal-Organic Chemical Vapour Deposition (MOCVD) [47], so an abrupt doping profile can be obtained by growing an n-doped segment on top of a p-doped one. However, one may expect that if the morphology of the p-doped segment is degraded by the Mg incorporation, the material quality of the top segment may be compromised.

In the present work we investigate this open question by comparing the electrical and optical properties of n-base and p-base p-n junction GaN NWs. The NWs are grown by PAMBE on Si (111) substrate using Mg and Si as doping sources. The NW morphology and optical properties are first assessed on a series of homogeneously Mg-doped samples. Then individual NWs containing n-base and p-base p-n junctions are analyzed by cathodoluminescence (CL) and EBIC. For the n-base junction, the analyses reveal a parasitic radial shell resulting in a mixed axial and radial behaviour and a high wire-to-wire inhomogeneity. When the doping order is inverted, purely axial junctions are achieved characterized by a lower wire-to-wire dispersion. The analysis of the EBIC profiles provides an estimate of the hole concentration in excess of 10^{18} cm^{-3}. For this high hole concentration, the NWs preserved a cylindrical morphology and exhibited good optical properties.

2. Nanowire growth

Self-assembled GaN NWs were grown on a conductive oxide-free Si(111) substrate by PAMBE, active nitrogen (N) being supplied by a radiofrequency plasma cell. Prior to the growth of GaN NWs, a 2.5 nm thick AlN buffer layer was deposited on the substrate [48, 49] to allow for a better control of the NW nucleation, density and orientation [50–54]. The GaN NW growth was performed under N-rich conditions with an N/Ga ratio of about 1.36, a high growth rate of 0.7 monolayers/sec and at a fixed substrate temperature of 800 °C. The n-type and p-type doping of GaN NWs was achieved by using Si and Mg, respectively, the doping level being modulated by adjusting the dopant cell temperature.

Two sets of samples were investigated. First, a series of five homogeneously p-type doped GaN NW samples was grown during 3 h under identical condition except for the doping level. The Mg cell temperature T_{Mg} was increased by increments of 50°C from 225°C to 425°C. In addition, an undoped reference NW sample and one homogeneously n-type doped NW sample using the Si cell temperature T_{Si} of 1150°C were grown.

The resulting doped GaN NWs are vertically oriented with a predominantly hexagonal shape. Figure 1 displays cross-sectional scanning electron microscopy (SEM) images of the undoped reference sample (panel a), p-doped GaN NWs with T_{Mg} of 375 °C and 425°C (panels b and c) and n-doped NWs (panel d). The average NW diameter for the undoped reference sample is 40 nm and the length is 1.1 µm. For the Si doped sample the NW morphology and in particular the diameter remain similar to the undoped case, while the average NW length is reduced to 0.86 µm. In the literature, the Si doping was reported to delay the NW nucleation and to reduce the axial growth rate [14], which is consistent with the observed length reduction. For very high doping levels, Si doping may lead to inverse tapering [14, 15] and even trumpet shape formation [55]. In our study, this high doping level was not reached and a cylindrical NW shape with a diameter close to the one in undoped reference was preserved.

For the Mg doped NWs an increase of the diameter is observed, which increases up to 80 nm for the higher doping cell temperature, while the average NW length slightly decreases to 1 µm. These observations are consistent with previous publications, where the Mg doping was reported to speed up the NW nucleation, while leading to a decrease in the NW growth rate and to a strong increase of the NW diameter [14]. It is important to note that up to a Mg temperature of 425 °C, the NWs preserve a cylindrical shape with only limited coalescence between adjacent NWs.

We note that it is difficult to precisely analyze the radial growth. It can be done by transmission electron microscopy

(TEM) by introducing AlN marker layers during the NW growth [48, 56, 57], however the marker layers create potential barriers and cannot be applied in samples dedicated to electrical measurements.

After morphological and optical analyses of Mg-doped NWs (detailed in the next section), a second set of two samples containing p-n junctions with a different doping order was grown. The Si cell temperature was fixed at 1150°C. For the Mg cell temperature the highest value T_{Mg} =425 °C was chosen. The "n-base" p-n junction consists of a bottom n-doped segment grown for 3 h and a top p-doped segment grown for 2 h. The "p-base" p-n junction consists of a bottom p-doped segment grown for 1.5 h and a top n-doped segment grown for 3 h. The Si(111) substrate was also changed from n-type to p-type to match the substrate doping type with the NW base doping type. The corresponding cross-sectional morphologies of the "n-base" and "p-base" p-n junctions are shown in Figure 1(e) and (f), respectively. Focusing first on the "n-base" p-n junction (figure 1(e)) one can notice a widening of the NWs in their upper part. Such sort of inverse tapering results from an enhancement of the radial growth induced by the Mg incorporation during the growth of the p-part [22, 23, 27, 39].

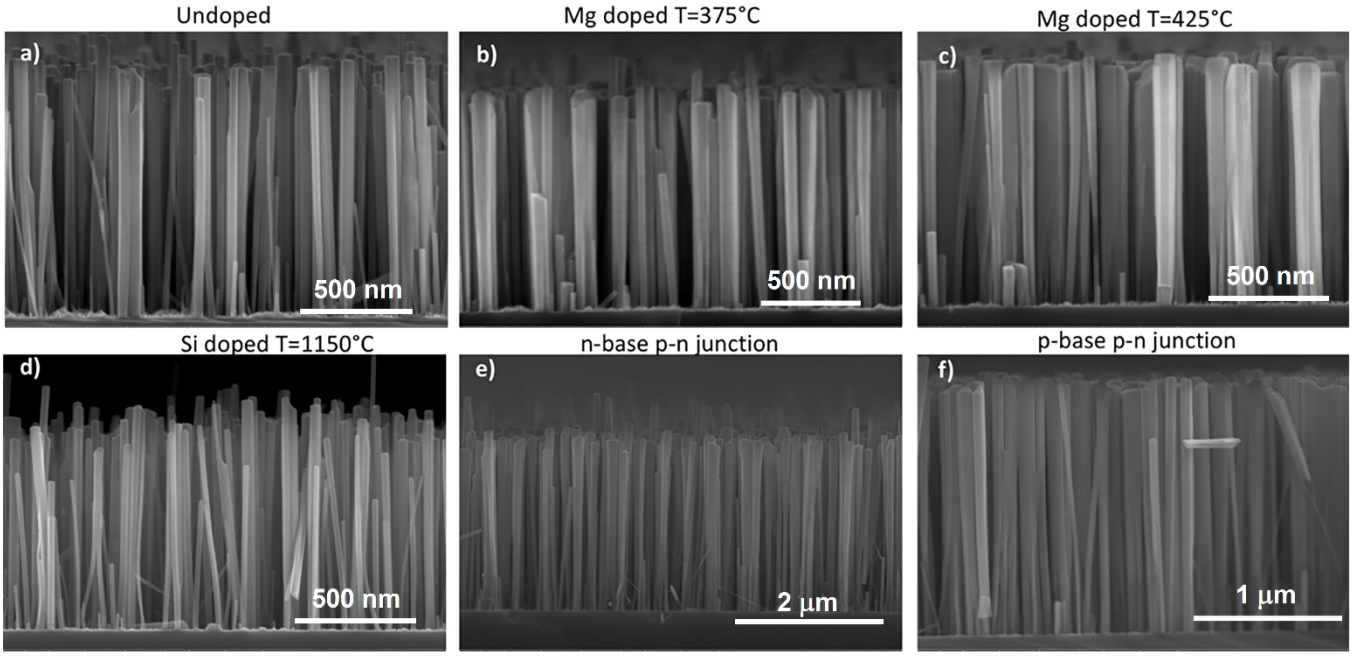

Figure 1. Cross-sectional SEM images of GaN NWs grown with different doping profiles. (a) Undoped NWs; (b) Mg-doped NWs with T_{Mg}=375°C; (c) Mg-doped NWs with T_{Mg}=425°C; (d) Si doped NWs with T_{Si}=1150°C; (e) n-base p-n junction NWs; (f) p-base p-n junction NWs.

For its "p-base" counterpart (figure 1(f)), although a mild coalescence can be found in the upper side, which is typical for long dense NWs, the shape of individual NWs has almost no inverse tapering.

3. Photoluminescence analyses of the nanowire ensembles

The optical properties of the p-doped GaN NW series and of the n-doped sample were investigated by low-temperature photoluminescence (PL) spectroscopy. The characterization was performed at 10 K by exciting the NW ensembles with a continuous-wave laser emitting at 266 nm. The laser was focused on the top surface of the NW ensembles to a spot of 3 μm diameter using an ultraviolet objective with a numerical aperture of 0.36. The PL spectra were analyzed in a 460 mm focal length grating spectrometer equipped with a liquid nitrogen cooled charge-coupled device (CCD) camera.

Figure 2(a) presents the PL spectra collected from the GaN NWs grown with different Mg cell temperatures. The signal was dispersed by a 600 grooves/mm grating, allowing for a spectral resolution of around 1 meV. For the sample grown with the lowest Mg cell temperature T_{Mg} = 225 °C, the spectra present a dominant near band edge (NBE) excitonic emission with a peak energy located at 3.47 eV. Two additional lower intensity peaks around 3.45 eV and 3.42 eV were also observed. The former one at 3.45 eV is well-known for nominally undoped GaN NWs grown on Si substrates, which is usually assigned to be the excitonic recombination in presence of inversion domain boundaries [58, 59]. The latter one at 3.42 eV can be associated with the recombination of excitons bound to plane stacking faults [60]. The NBE emission exceeds by two orders of magnitude any residual signal in the 3.0-3.3 eV energy band, so for the lowest Mg cell temperature no optical features evidencing the p-doping could be observed. We note that the spectrum of the n-doped NW

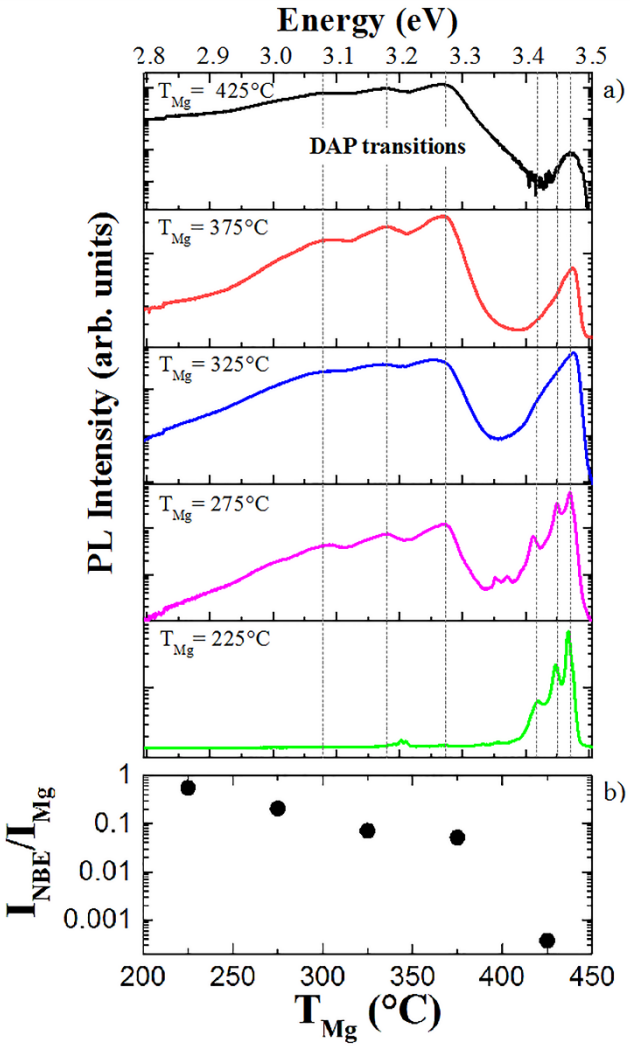

Figure 2. (a) – Low-temperature PL spectra in logarithmic scale of p-doped GaN NWs grown with different TMg. (b) – The integrated emission intensity ratio I_{NBE}/I_{Mg} in logarithmic scale as a function of T_{Mg}.

sample (figure 1S in supplementary material) presents similar features as the T_{Mg} = 225 °C doped sample, namely the D^0X_A excitonic line and a strong emission from inversion domain boundaries at 3.45 eV.

With the increase of the Mg cell temperature in p-doped NWs, the NBE emission peaks broaden and merge into one asymmetric peak starting from T_{Mg} = 325°C. Moreover, a wide emission band peaked around 3.27 eV together with its phonon replicas starts to show up at T_{Mg} = 275 °C, which is associated with the donor-acceptor pair (DAP) transitions. At larger T_{Mg}, the DAP emission becomes preponderant while the NBE emission weakens. For T_{Mg} = 425 °C, the DAP intensity exceeds the NBE by two orders of magnitude.

The observed modification of the spectral shape points to the increase of the Mg incorporation in the GaN NWs with increasing T_{Mg}. It has been reported [23] that the relative intensity of the DAP emission can be used to estimate the p-doping. In the following, the integrated intensity of the emission from the Mg-related DAP transitions is referred to as I_{Mg} and the integrated intensity of the rest of the NBE transitions is called I_{NBE}.

By plotting the ratio of the I_{NBE} by I_{Mg} as a function of the Mg cell temperature, we find a quasi-linear relationship in semi-logarithmic scale between I_{NBE}/I_{Mg} and T_{Mg}, as depicted in figure 2(b). The value of I_{NBE}/I_{Mg} decreases from 0.55 for T_{Mg} = 225 °C down to 3.75×10^{-4} for T_{Mg} = 425 °C. Similar range of I_{NBE}/I_{Mg} was reported for GaN NWs in ref. [23], where the hole concentration in GaN NWs was quantified by using photoelectrochemical methods and correlated with the optical signatures.

Applying their calibration, the hole concentration in our NWs can be estimated as approx. 6.0×10^{17} cm^{-3} for T_{Mg} = 225 °C going up to approx. 1.2×10^{18} cm^{-3} for T_{Mg} = 425 °C. We note that this high hole concentration is achieved for morphologies preserving the NW shape while the morphological degradation happens for higher Mg fluxes. For the same hole concentration, the NW shape reported in previous studies is much more affected by radial growth and coalescence [23]. We speculate that the better NW morphology for high Mg-doping in our investigation may be due to the high growth rate of 0.7 monolayers/sec, which modifies the growth kinetics.

4. Cathodoluminescence analyses of the p-n junction individual nanowires

The optical properties of the p-n junction NWs were analyzed by CL. To enable spatially resolved measurements, the NWs were dispersed on a silicon substrate. The experiments were performed in an Attolight Chronos microscope, recording the luminescence with an Andor Newton 920 CCD camera (1024×256 pixels, pixel width 26 µm) installed on a Horiba iHR320 dispersive spectrometer with 150/500 grating. The spectral resolution for the GaN NBE is estimated to be 2.3 nm. The measurements were performed at 10 K with an acceleration voltage of 6 kV and impinging current of ~10 nA.

Figure 3 displays CL spectra of individual p-n junction NWs with the n-base (panel (a)) and the p-base (panel (b)). The spectra are integrated over the NW length. In both spectra, DAP and NBE contributions are observed in agreement with the presence of n-doped and p-doped regions, however the relative intensity of the two peaks is different. For the n-base p-n junction NW, the intensity of the DAP transition (highlighted in red in figure 3) dominates the spectrum, while

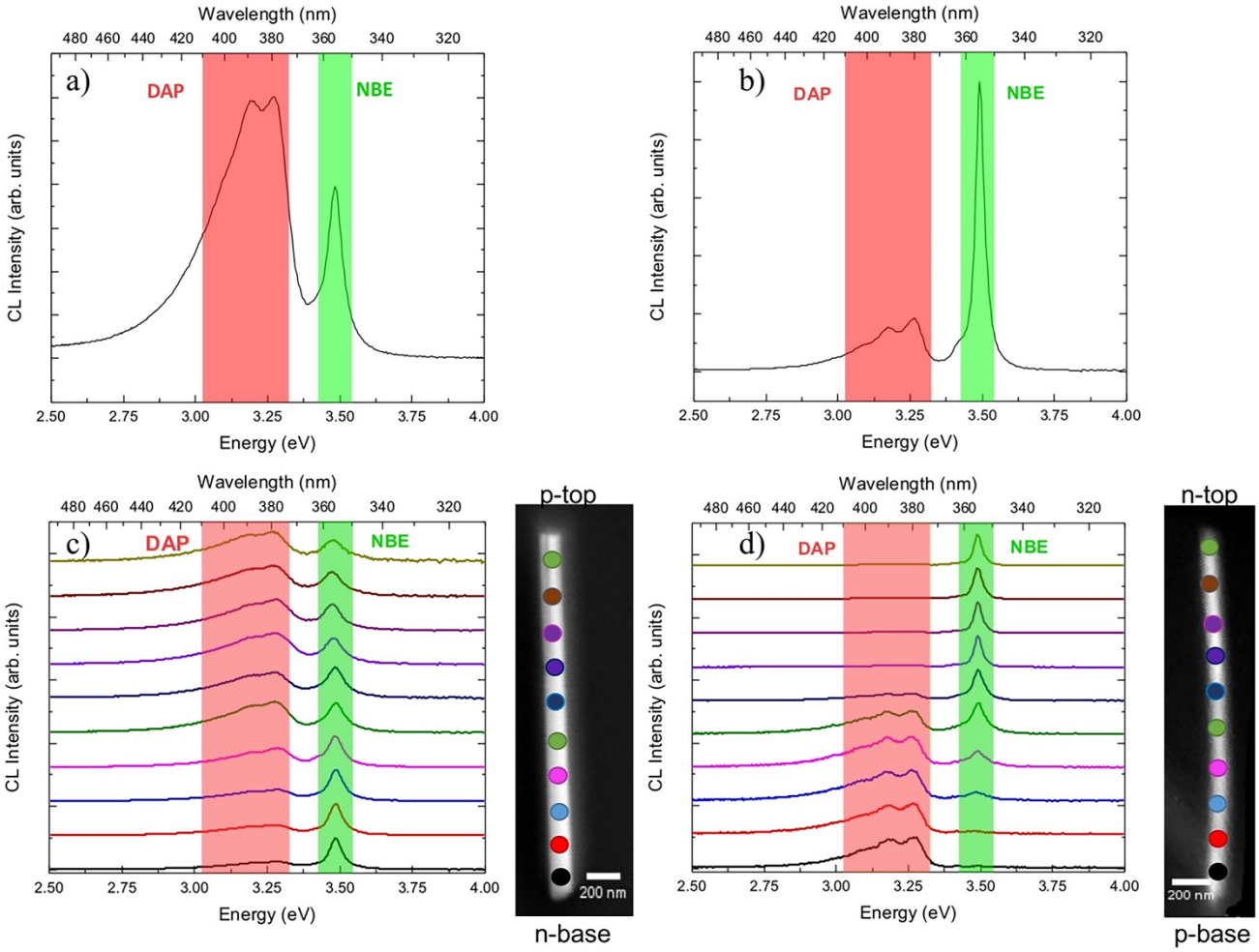

Figure 3. CL spectra of (a) n-base and (b) p-base single NW p-n junctions at 10 K. Normalized CL spectra for different excitation points along the NW axis for (c) n-base and (d) p-base NW junction. Color bands highlight the NBE (green) and the DAP (red) spectral ranges. The insets show SEM images acquired simultaneously with CL spectra showing the excitation positions corresponding to spectra in (c) and (d).

for the p-base junction NW the spectrum is dominated by the NBE transition (highlighted in green in figure 3). This change of the relative intensity points to the higher volume of the p-doped material in n-base p-n junction NWs. The full-width-at-half-maximum (FWHM) of the NBE peak also differs: it is equal to 10 meV for the n-base junction and to 5 meV for the p-base junction.

To analyze the localization of the two contributions, CL spectra in different regions were examined. Figure 3(c) shows the normalized CL spectra at different points along the NW axis from the bottom to the top for the n-base NW junction. The excitation positions are indicated on the corresponding SEM image in the inset. It is observed that a strong DAP emission is present everywhere along the wire axis. The DAP completely dominates over the NBE in the top p-doped segment and slowly decreases in the n-doped base segment. The NBE peak is broad with a FWHM close to 10 meV over the entire NW length. The observed presence of the DAP peak over the entire NW length may be understood if we suppose that a p-doped shell is present around the n-doped base. This hypothesis will be further supported by EBIC investigation discussed in the next section.

The same analyses were performed for the p-base junction NW as shown in figure 3(d). The DAP emission also dominates over the NBE in the bottom p-doped segment. However, in the top n-doped segment the GaN NBE emission becomes preponderant. The broadening of the NBE peak narrows towards the NW top going from 10 meV in the lower part to 5 meV in the top n-doped segment. These observations are consistent with the nominal structure of the p-base junction NW.

5. EBIC characterization of GaN n-base and p-base p-n junction nanowires

Hitachi SU8000 SEM microscope equipped with a Kleindiek micro probe-station composed of 4 mobile nano-

probes was used for the NW analyses. All EBIC measurements were made using the acceleration voltage of 10 kV and the impinging current of 60 pA [61, 62]. To perform single NW EBIC measurements, the sample is cleaved without disconnecting the NWs from their substrate and the cross section is exposed to the electron beam. The individual NWs are contacted on their top by a nano-probe, while the bottom contact is provided by the substrate connected to the ground. To measure the induced current, a low noise current preamplifier SR570 coupled with a Gatan Digiscan system is used. The EBIC map is constructed point by point by scanning the sample surface.

First the n-base p-n junction NWs were analyzed. Figure 4 presents the NW schematic (panel a)), examples of EBIC maps of different NWs (panels b) – e)) as well as an example of a single NW current-voltage (I-V) characteristic recorded with a blanked electron beam (panel f)). The EBIC maps reveal the junction activity as a bright contrast. The I-V curve presents a typical diode-like shape with the opening voltage around 3.5 V in agreement with the expected p-n junction structure of the NW. The leakage current remains low for reverse biases up to -5 V.

We note that the EBIC signal from the NW junctions is weak or absent without external bias (cf. figure S2 in Supplementary Material showing the EBIC maps under different external biases). This is attributed to the presence of a Schottky barrier between the NW and the nano-manipulator. Indeed, for a forward bias, a dark contrast is observed in the vicinity of the contact point (cf. figure S2 in Supplementary Material), proving the Schottky nature of the contact [62]. This Schottky barrier can be flattened by applying a negative bias thus revealing the p-n junction signal.

Figure 4(b), (c), (d) and (e) displays SEM images and the corresponding EBIC maps under -5 V external bias for four individual NWs. A strong difference is observed with respect to the nominal NW structure schematically illustrated in figure 4(a). The junction signal is markedly displaced toward the substrate with respect to the expected position of the junction according to the growth rate calibration. In addition, the EBIC signal shows an irregular shape, which does not correspond to the one expected for an axial junction NW. The signal position and shape strongly vary from wire to wire. In particular, the extension of the region producing the induced current varies from 400 nm up to 1 µm.

These observations deviating from the nominal NW structure can be explained by the parasitic radial growth, which is enhanced in presence of Mg dopants. During the growth of the Mg-doped upper segment, the lateral overgrowth leads to the lateral deposition of a p-doped shell around the n-doped NW base. This shell has an irregular shape [48, 63] which depends on the local environment of the NW due to shadow effects or eventual coalescence of the neighbouring NWs. As a result, a mixed axial and core-shell p-n junction is formed in the NWs, which explains the extended irregular EBIC signal and the difficulty to define the position of the junction. The hypothesis of a p-doped parasitic shell is coherent with the previously described CL results, which showed a strong DAP signal not only in the top p-doped part, but also in the bottom n-doped segment.

The growth analyses have suggested that the problem of the radial parasitic growth can be reduced by inverting the doping order. To test this hypothesis, p-base NW junctions were analyzed under the same experimental conditions. Figure 5 presents an example of a single NW EBIC map and an I-V curve for a representative p-base NW junction (other examples confirming good wire-to-wire reproducibility are shown in figure S3 of Supplementary Materials). The p-n junction signal in p-base NWs is given by a dark contrast in EBIC maps, which reflects the opposite direction of the built-in field and thus of the induced current compared to the n-base wires, as expected for the inverted doping order. The change of the doping order also results in the I-V curve inversion as illustrated in figure 5(c). We note that the absolute value of the current in the I-V curve is reduced compared to the n-base NW (cf. Fig. 4(f)) which may be related to the difference in the junction area between these two cases: a mixed axial and core/shell junction in the n-base NWs and a purely axial junciton in the p-base NWs.

The EBIC signal from the junction was observed under an external bias above 1 V (for this doping order, positive bias corresponds to the reversely polarized p-n junction). No signal was observed without an external bias, which may be attributed either to the Schottky contact with the nano-manipulator or to the potential barrier at the NW/substrate interface. (Indeed, for some NWs, an induced current was observed close to the substrate indicating that the carrier collection may be difficult through the p-GaN/p-Si interface.)

The EBIC signal of the junction in p-base NWs has a regular shape, which is reproducible between different NWs (cf. figure S3 in Supplementary Materials). The junction location can be approximated by the maximum of the induced current, its position is similar for different NWs and corresponds to the nominal one.

The regular shape of the EBIC signal in the p-base NW junction shows that contrary to the n-base NWs, it behaves as a regular axial junction. We cannot completely exclude the parasitic radial growth during the deposition of the top Si-doped segment, however it should be much weaker than for the case of a p-doped top segment. This is consistent with the cylindrical morphology of Si-doped NWs as described in the growth section. The EBIC does not reveal any electrical activity of this hypothetical n-doped shell, therefore, if this latter exists it should be depleted.

Thanks to the regular shape of the EBIC signal, p-base NW junctions can be used for doping estimation. The doping concentration can be assessed using the model proposed by

Tchoulfian et al. [64], in which the EBIC profile is analyzed to extract the depletion region width. By fitting the signal decay, the minority carrier's diffusion lengths can also be estimated. The analyses of a typical EBIC profile along the NW axis collected under reverse bias of 2 V are illustrated in figure 6(a). The EBIC profile can be divided into three parts: the diffusion current in the p region, the diffusion current in the n region and the drift current in the space charge region. The induced current is theoretically modelled as a convolution of the generation function with the probability of charge collection. This latter can be approximated to unity in the depletion layer, elsewhere the collection probability can be written as:

$$Q(x) = e^{-\frac{x}{L_d}}, \quad (1)$$

where L_d is the diffusion length of the corresponding minority carriers [62]. Based on this expression the minority carrier diffusion lengths are extracted by the exponential fitting of the decay of the current from either side of the depletion region edge. By analyzing different NWs, the electron diffusion length in the p-doped region is estimated to be 59 ± 6 nm, while the hole diffusion length in the n-doped segment is 49 ± 5 nm. Compared to the literature reports for n-base p-n junction NWs [22] (giving values 40 - 77 nm for holes and 122 - 170 nm for electrons), the hole diffusion length in our NWs is comparable, while the electron diffusion length is shorter.

The space charge region can be estimated as the part of the NW where the EBIC profile deviates from the exponential decay [64]. By analyzing several NWs, the space charge region is extracted to be equal to 65 ± 6 nm. To estimate the electron and hole concentrations we need to measure the depletion region extension in the n- and p-doped parts of the junction, which requires a precise knowledge of the junction position. To localize the interface between the p- and n-doped segments, a common method is to analyze the secondary electron contrast which depends on the doping type [62]. However, in the present case the NWs are very thin and the contrast difference between the p- and n-doped parts is insufficient to localize the junction interface with precision. The junction position may be estimated by searching the maximum of the EBIC profile, however this method can be erroneous especially in the case when the space charge region is narrow and its extension is comparable with the beam/matter interaction volume. For these reasons, we should not rely on the EBIC peak position and the electron and hole concentrations cannot be separately extracted from the present EBIC experiments. However, we can estimate their minimal values and their respective dependence. The correlation between the electron and the hole concentrations is obtained

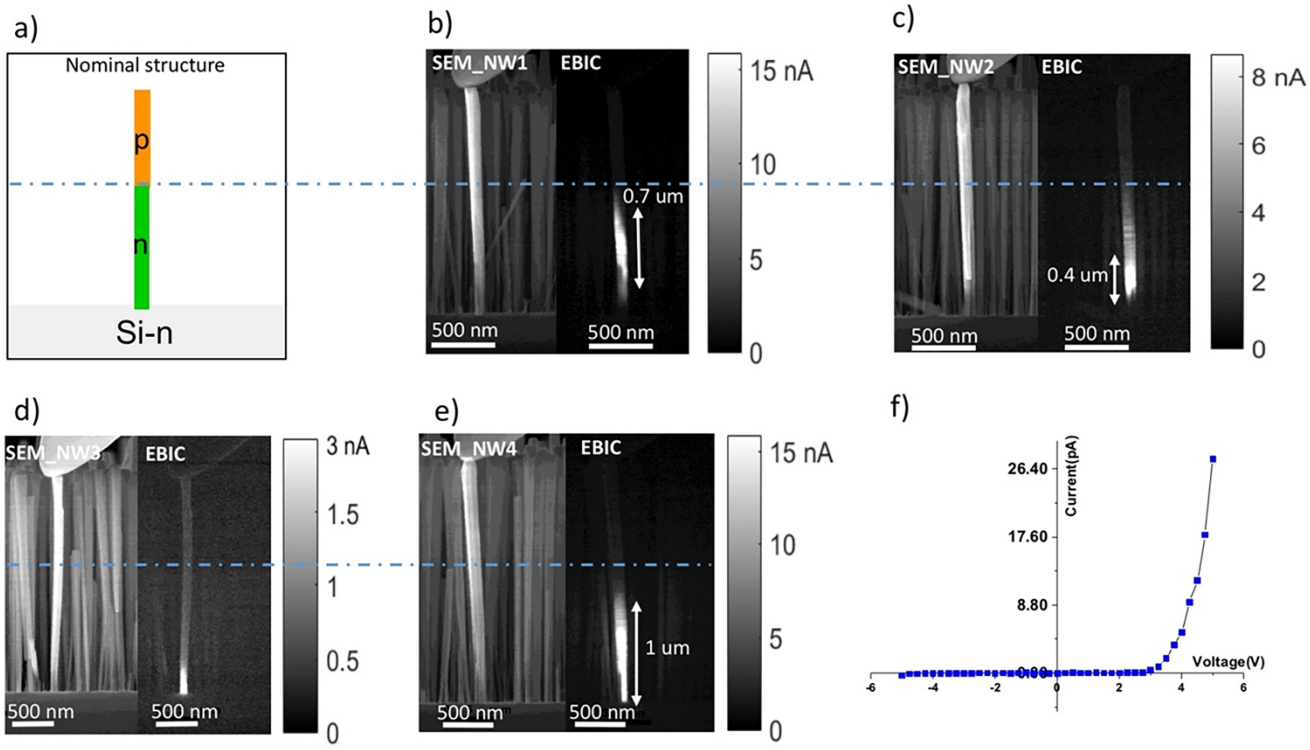

Figure 4. (a) – Schematic of an n-base NW p-n junction showing the expected position of the junction. (b), (c), (d) and (e) – SEM images and the corresponding EBIC maps of four different NWs. (f) – Single NW I-V curve recorded with a blanked beam.

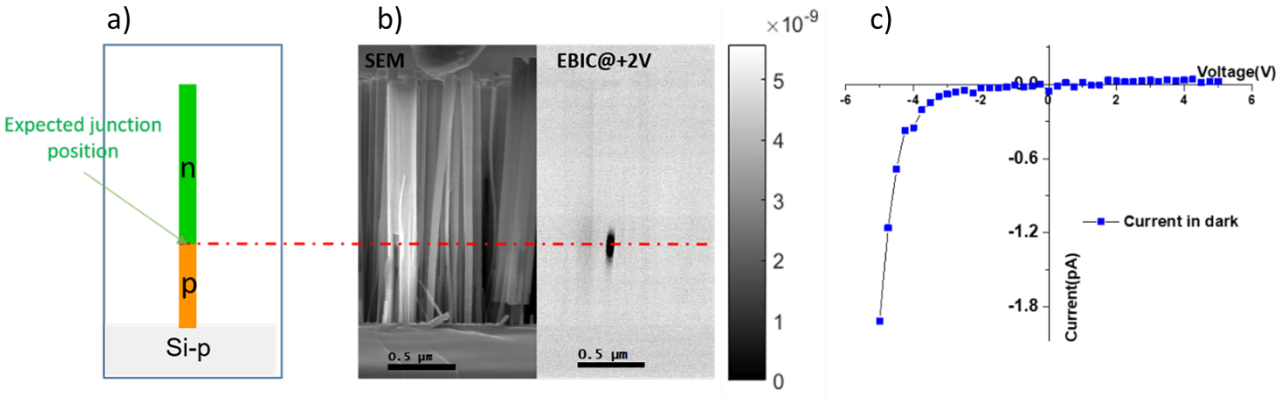

Figure 5. (a) – Schematic of a p-base NW junction. (b) – SEM image of an individual NW and the corresponding EBIC map under +2 V. (c) – Single NW I-V curve recorded with a blanked beam.

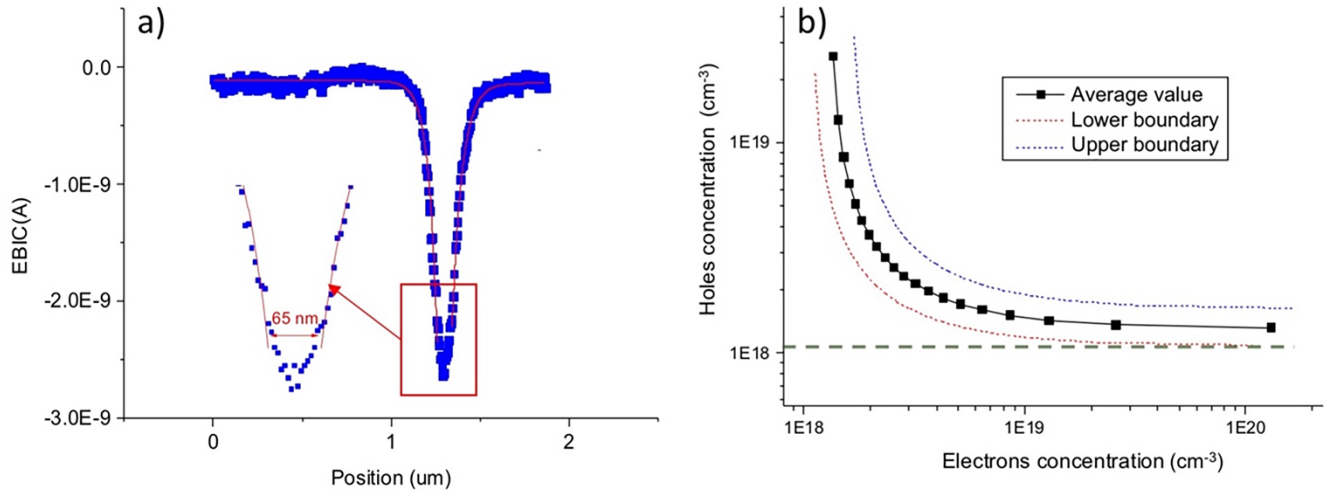

Figure 6. (a) – EBIC profile along the NW axis under reverse (+2 V) bias and the exponential fit of the current decay (inset shows a close-up on the induced current peak); (b) – Extracted hole concentration as a function of the electron concentration. The dashed line shows the lowest limit of the hole concentration.

by assuming the interface coordinate in different positions along the space charge region starting from x_p (coordinate of the space charge region boundary with the p-doped segment) to x_n (coordinate of the space charge region boundary with the n-doped segment). x_n and x_p are determined as positions at which the EBIC profile deviates from the exponential decrease in the p- and n-doped segments of the junction. For each assumed junction position, the carrier concentrations are calculated using the electrostatic model of the p-n junction as detailed in [62]. The computed electron and hole concentrations are plotted in figure 6(b).

Considering the error bars on the xn and xp values extracted from the experimental profile, for each electron concentration the lowest, the highest and the average hole concentrations are traced. The lowest limit for the hole (electron) concentration is determined as the horizontal (vertical) asymptote of the curves. These limits correspond to the hypothesis that the full space charge region is located in the p-doped (n-doped) segment. The lowest limit for the hole concentration corresponds to 10^{18} cm^{-3}, while the actual concentration can be higher.

The optical estimation described in section 3 for the Mg cell temperature of 425 °C used for the p-n junction growth yielded hole concentration of 1.2×10^{18} cm^{-3}. Therefore, the low boundary for the hole concentration obtained from EBIC analyses is compatible with the estimation based on the PL spectra. It is important to note that this high hole concentration is achieved without deterioration of the NW morphology.

Conclusions

In conclusion, the electrical and optical properties of n-base and p-base p-n junctions in PAMBE grown GaN NWs were investigated. For the n-base junctions, a parasitic radial shell accompanying the top p-doped segment growth results in a mixed axial and radial behaviour and a large wire-to-wire

inhomogeneity. Abrupt purely axial p-n junctions with a good wire-to-wire reproducibility are demonstrated for an inverted doping order, which is favourable for axial NW devices such as photodetectors or LEDs. An active hole concentration in the 10^{18} cm^{-3} range was achieved without degrading the wire morphology.

Acknowledgements

This work was financially supported by EU H2020 ERC project "NanoHarvest" (grant no. 639052), the ITN Marie Curie project INDEED (grant no. 722176), by the Labex GANEX (grant no. ANR-11-LABX-0014), by the Region Ile-de-France in the framework of C'Nano IdF and by the European Union (FEDER 2007-2013).

ORCID iD

Stéphane Collin https://orcid.org/0000-0001-6176-1653
Andrey Babichev https://orcid.org/0000-0002-3463-4744
Jean-Christophe Harmand https://orcid.org/0000-0003-0758-0389
François H. Julien https://orcid.org/0000-0003-4308-6361
Maria Tchernycheva https://orcid.org/0000-0003-4144-0793

References

[1] Amano H, Kito M, Hiramatsu K and Akasaki I 1989 P-Type Conduction in Mg-Doped GaN Treated with Low-Energy Electron Beam Irradiation (LEEBI) *Jpn. J. Appl. Phys*. **28** L2112–4
[2] Akasaki I, Amano H, Kito M and Hiramatsu K 1991 Photoluminescence of Mg-doped p-type GaN and electroluminescence of GaN p-n junction LED *J. Lumin.* **48-49** 666–70
[3] Nakamura S, Mukai T, Senoh M and Iwasa N 1992 Thermal Annealing Effects on P-Type Mg-Doped GaN Films *Jpn. J. Appl. Phys.* **31** L139–42
[4] Feezell D and Nakamura S 2018 Invention, development, and status of the blue light-emitting diode, the enabler of solid-state lighting *C. R. Phys.* **19** 113–33
[5] Wang H and Chen A-B 2000 Calculation of shallow donor levels in GaN *J. Appl. Phys.* **87** 7859–63
[6] Alves H, Böhm M, Hofstaetter A, Amano H, Einfeldt S, Hommel D, Hofmann D M and Meyer B K 2001 Compensation mechanism in MOCVD and MBE grown GaN:Mg *Phys. B* **308-310** 38–41
[7] Iida D, Tamura K, Iwaya M, Kamiyama S, Amano H and Akasaki I 2010 Compensation effect of Mg-doped a- and c-plane GaN films grown by metalorganic vapor phase epitaxy *J. Cryst. Growth* **312** 3131–5
[8] Pernot J, Donatini F and Tchoulfian P 2014 Doping and Transport *Wide Band Gap Semiconductor Nanowires 1: Low-Dimensionality Effects and Growth* **5** 99–123 http://dx.doi.org/10.1002/9781118984321.ch5
[9] Kirste R, Hoffmann M P, Tweedie J, Bryan Z, Callsen G, Kure T, Nenstiel C, Wagner M R, Collazo R, Hoffmann A and Sitar Z 2013 Compensation effects in GaN:Mg probed by Raman spectroscopy and photoluminescence measurements *J. Appl. Phys.* **113** 103504
[10] Flynn C and Lee W 2014 The dependence of Raman scattering on Mg concentration in Mg-doped GaN grown by MBE. *Mater. Res. Express* **1** 025901
[11] Tchernycheva M, Sartel C, Cirlin G, Travers L, Patriarche G, Harmand J-C, Dang L S, Renard J, Gayral B, Nevou L and Julien F 2007 Growth of GaN free-standing nanowires by plasma-assisted molecular beam epitaxy: structural and optical characterization *Nanotechnology* **18** 385306
[12] Wölz M, Hauswald C, Flissikowski T, Gotschke T, Fernández-Garrido S, Brandt O, Grahn H T, Geelhaar L and Riechert H 2015 Epitaxial Growth of GaN Nanowires with High Structural Perfection on a Metallic TiN Film. *Nano Lett.* **15** 3743–47
[13] Kumaresan V, Largeau L, Oehler F, Zhang H, Mauguin O, Glas F, Gogneau N, Tchernycheva M and Harmand J-C 2016 Self-induced growth of vertical GaN nanowires on silica. *Nanotechnology* **27** 135602
[14] Furtmayr F, Vielemeyer M, Stutzmann M, Arbiol J, Estradé S, Peirò F, Morante J R and Eickhoff M 2008 Nucleation and growth of GaN nanorods on Si (111) surfaces by plasma-assisted molecular beam epitaxy - The influence of Si- and Mg-doping *J. Appl. Phys.* **104** 034309
[15] Stoica T and Calarco R 2011 Doping of III-Nitride Nanowires Grown by Molecular Beam Epitaxy *IEEE J. Sel. Top. Quantum Electron.* **17** 859–68
[16] Schuster F, Winnerl A, Weiszer S, Hetzl M, Garrido J A and Stutzmann M 2015 Doped GaN nanowires on diamond: Structural properties and charge carrier distribution *J. Appl. Phys*. **117** 044307
[17] Limbach F, Caterino R, Gotschke T, Stoica T, Calarco R, Geelhaar L and Riechert H 2012 The influence of Mg doping on the nucleation of self-induced GaN nanowires *AIP Adv.* **2** 012157
[18] Sutter E 2010 Morphology and Optical Properties of Mg Doped GaN Nanowires in Dependence of Growth Temperature *J. Optoelectron. Adv. Mater.*, **12** BNL-93776-2010-JA
[19] Zhao S and Mi Z 2017 Recent Advances on p-Type III-Nitride Nanowires by Molecular Beam Epitaxy *Crystals* **7** 268
[20] Fang Z, Robin E, Rozas-Jiménez E, Cros A, Donatini F, Mollard N, Pernot J and Daudin B 2015 Si Donor Incorporation in GaN Nanowires *Nano Lett.* **15** 6794–801
[21] Siladie A-M, Amichi L, Mollard N, Mouton I, Bonef B, Bougerol C, Grenier A, Robin E, Jouneau P-H, Garro N, Cros A and Daudin B 2018 Dopant radial inhomogeneity in Mg-doped GaN nanowires *Nanotechnology* **29** 255706
[22] Fang Z, Donatini F, Daudin B and Pernot J 2017 Axial p–n junction and space charge limited current in single GaN nanowire *Nanotechnology* **29** 01LT01
[23] Kamimura J, Bogdanoff P, Ramsteiner M, Corfdir P, Feix F, Geelhaar L and Riechert H 2017 p-Type Doping of GaN Nanowires Characterized by Photoelectrochemical Measurements *Nano Lett.* **17** 1529–37
[24] Siladie A-M, Jacopin G, Cros A, Garro N, Robin E, Caliste D, Pochet P, Donatini F, Pernot J and Daudin B 2019 Mg and In Codoped p-type AlN Nanowires for pn Junction Realization *Nano Lett.* **19** 8357–64

[25] Zhao S, Connie A T, Dastjerdi M H T, Kong X H, Wang Q, Djavid M, Sadaf S, Liu X D, Shih I, Guo H and Mi Z 2015 Aluminum nitride nanowire light emitting diodes: Breaking the fundamental bottleneck of deep ultraviolet light sources *Sci. Rep.* **5** 8332

[26] Connie A T, Zhao S, Sadaf S M, Shih I, Mi Z, Du X, Lin J and Jiang H 2015 Optical and electrical properties of Mg-doped AlN nanowires grown by molecular beam epitaxy *Appl. Phys. Lett.* **106** 213105

[27] Wang Q, Liu X, Kibria M G, Zhao S, Nguyen H P T, Li K H, Mi Z, Gonzalez T and Andrews M P 2014 p-Type dopant incorporation and surface charge properties of catalyst-free GaN nanowires revealed by micro-Raman scattering and X-ray photoelectron spectroscopy *Nanoscale* **6** 9970–6

[28] Tran N H, Le B H, Zhao S and Mi Z 2017 On the mechanism of highly efficient p-type conduction of Mg-doped ultra-wide-bandgap AlN nanostructures *Appl. Phys. Lett.* **110** 032102

[29] Storm K, Halvardsson F, Heurlin M, Lindgren D, Gustafsson A, Wu P M, Monemar B and Samuelson L 2012 Spatially resolved Hall effect measurement in a single semiconductor nanowire *Nat. Nanotechnol.* **7** 718–22

[30] Hultin O, Otnes G, Borgström M T, Björk M, Samuelson L and Storm K 2015 Comparing Hall Effect and Field Effect Measurements on the Same Single Nanowire *Nano Lett.* **16** 205–11

[31] Haas F, Zellekens P, Lepsa M, Rieger T, Grützmacher D, Lüth H and Schäpers T 2016 Electron Interference in Hall Effect Measurements on GaAs/InAs Core/Shell Nanowires *Nano Lett.* **17** 128–35

[32] Gîrgel I, Šatka A, Priesol J, Coulon P-M, Le Boulbar E D, Batten T, Allsopp D W E and Shields P A 2018 Optical characterization of magnesium incorporation in p-GaN layers for core–shell nanorod light-emitting diodes *J. Phys. D: Appl. Phys.* **51** 155103

[33] Hortelano V, Martínez O, Cuscó R, Artús L and Jiménez J. 2016 Cathodoluminescence study of Mg activation in non-polar and semi-polar faces of undoped/Mg-doped GaN core–shell nanorods *Nanotechnology* **27** 095706

[34] Mohajerani M S, Khachadorian S, Schimpke T, Nenstiel C, Hartmann J, Ledig J, Avramescu A, Strassburg M, Hoffmann A and Waag A 2016 Evaluation of local free carrier concentrations in individual heavily-doped GaN:Si micro-rods by micro-Raman spectroscopy *Appl. Phys. Lett.* **108** 091112

[35] Kumar R, Nayak S and Shivaprasad S M 2019 Spectroscopic signatures of native charge compensation in Mg doped GaN nanorods *Mater. Res. Express* **6** 105911

[36] Wang F, Gao Q, Peng K, Li Z, Li Z, Guo Y, Fu L, Smith L M, Tan H H and Jagadish C 2015 Spatially Resolved Doping Concentration and Nonradiative Lifetime Profiles in Single Si-Doped InP Nanowires Using Photoluminescence Mapping *Nano Lett.* **15** 3017–23

[37] Chen H-L, Himwas C, Scaccabarozzi A, Rale P, Oehler F, Lemaître A, Lombez L, Guillemoles J-F, Tchernycheva M, Harmand J-C, Cattoni A and Collin S 2017 Determination of n-Type Doping Level in Single GaAs Nanowires by Cathodoluminescence. *Nano Lett.* **17** 6667–75

[38] Tchoulfian P, Donatini F, Levy F, Amstatt B, Dussaigne A, Ferret P, Bustarret E and Pernot J 2013 Thermoelectric and micro-Raman measurements of carrier density and mobility in heavily Si-doped GaN wires *Appl. Phys. Lett.* **103** 202101

[39] Minj A, Cros A, Auzelle T, Pernot J and Daudin B 2016 Direct assessment of p–n junctions in single GaN nanowires by Kelvin probe force microscopy *Nanotechnology* **27** 385202

[40] Brubaker M D, Blanchard P T, Schlager J B, Sanders A W, Herrero A M, Roshko A, Duff S M, Harvey T E, Bright V M, Sanford N A and Bertness K A 2013 Toward Discrete Axial p–n Junction Nanowire Light-Emitting Diodes Grown by Plasma-Assisted Molecular Beam Epitaxy *J. Electron. Mater.*, **42** 868–74

[41] Golam Sarwar A T M, Carnevale S D, Kent T F, Yang F, McComb D W and Myers R C 2015 Tuning the polarization-induced free hole density in nanowires graded from GaN to AlN *Appl. Phys. Lett.* **106** 032102

[42] De Luna Bugallo A, Tchernycheva M, Jacopin G, Rigutti L, Julien F H, Chou S-T, Lin Y-T, Tseng P-H and Tu L-W 2010 Visible-blind photodetector based on p–i–n junction GaN nanowire ensembles *Nanotechnology* **21** 315201

[43] Jacopin G, De Luna Bugallo A, Rigutti L, Lavenus P, Julien FH, Lin Y-T, Tu L-W, Tchernycheva M 2014 Interplay of the photovoltaic and photoconductive operation modes in visible-blind photodetectors based on axial p-i-n junction GaN nanowires. *Appl. Phys. Lett.* **104** 023116

[44] Cuesta S, Spies M, Boureau V, Donatini F, Hocevar M, den Hertog M I and Monroy E 2019 Effect of Bias on the Response of GaN Axial p–n Junction Single-Nanowire Photodetectors *Nano Lett.* **19** 5506–14

[45] Guan N, Dai X, Julien F H, Eymery J, Durant C and Tchernycheva M 2019 Nitride Nanowires for Light Emitting Diodes *Light-Emitting Diodes. Materials, Processes, Devices and Applications* 425–84

[46] Ra Y-H and Lee C-R 2019 Understanding the p-Type GaN Nanocrystals on InGaN Nanowire Heterostructures *ACS Photonics* **6** 2397–404

[47] Smorchkova I P, Haus E, Heying B, Kozodoy P, Fini P, Ibbetson J P, Keller S, DenBaars S P, Speck J S and Mishra U K 2000 Mg doping of GaN layers grown by plasma-assisted molecular-beam epitaxy *Appl. Phys. Lett.* **76** 718–20

[48] Tchernycheva M, Sartel C, Cirlin G, Travers L, Patriarche G, Harmand J-C, Dang L S, Renard J, Gayral B, Nevou L and Julien F Growth of GaN free-standing nanowires by plasma-assisted molecular beam epitaxy: structural and optical characterization *Nanotechnology* **18** 385306

[49] Largeau L, Galopin E, Gogneau N, Travers L, Glas F and Harmand J-C 2012 N-Polar GaN Nanowires Seeded by Al Droplets on Si(111) *Cryst. Growth Des.* **12** 2724–9

[50] Li S and Waag A 2012 GaN based nanorods for solid state lighting *J. Appl. Phys.* **111** 071101

[51] Landré O, Fellmann V, Jaffrennou P, Bougerol C, Renevier H, Cros A and Daudin B 2010 Molecular beam epitaxy growth and optical properties of AlN nanowires *Appl. Phys. Lett.* **96** 061912

[52] Brubaker M D, Levin I, Davydov A V, Rourke D M, Sanford N A, Bright V M and Bertness K A 2011 Effect of AlN buffer layer properties on the morphology and polarity of GaN nanowires grown by molecular beam epitaxy *J. Appl. Phys.* **110** 053506

[53] Songmuang R, Landré O and Daudin B 2007 From nucleation to growth of catalyst-free GaN nanowires on thin AlN buffer layer *Appl. Phys. Lett.* **91** 251902
[54] Bertness K A, Roshko A, Mansfield L M, Harvey T E and Sanford N A 2007 Nucleation conditions for catalyst-free GaN nanowires *J. Cryst. Growth* **300** 94–9
[55] Bolshakov A D, Mozharov A M, Sapunov G A, Shtrom I V, Sibirev N V, Fedorov V V, Ubyivovk E V and Mukhin I S 2018 Dopant-stimulated growth of GaN nanotube-like nanostructures on Si(111) by molecular beam epitaxy *Beilstein J. Nanotechnol.* **9** 146–54
[56] Tchernycheva M, Sartel C, Cirlin G, Travers L, Patriarche G, Largeau L, Mauguin O, Harmand J-C, Dang L S, Renard J, Gayral B, Nevou L and Julien F 2008 GaN/AlN free-standing nanowires grown by molecular beam epitaxy *Phys. Status Solidi C* **5** 1556–58
[57] Galopin E, Largeau L, Patriarche G, Travers L, Glas F and Harmand J C 2011 Morphology of self-catalyzed GaN nanowires and chronology of their formation by molecular beam epitaxy *Nanotechnology* **22** 245606
[58] Auzelle T, Haas B, Den Hertog M, Rouvière J-L, Daudin B and Gayral B 2015 Attribution of the 3.45 eV GaN nanowires luminescence to inversion domain boundaries *Appl. Phys. Lett.* **107** 051904
[59] Pfüller C, Corfdir P, Hauswald C, Flissikowski T, Kong X, Zettler J K, Fernández-Garrido S, Doğan P, Grahn H T, Trampert A, Geelhaar L and Brandt O 2016 Nature of excitons bound to inversion domain boundaries: Origin of the 3.45-eV luminescence lines in spontaneously formed GaN nanowires on Si(111) *Phys. Rev. B* **94** 155308
[60] Lähnemann J, Jahn U, Brandt O, Flissikowski T, Dogan P and Grahn H T Luminescence associated with stacking faults in GaN *J. Phys. D: Appl. Phys.* **47** 423001
[61] Piazza V, Wirths S, Bologna N, Ahmed AA, Bayle F, Schmid H, Julien F and Tchernycheva M 2019 Nanoscale analysis of electrical junctions in InGaP nanowires grown by template-assisted selective epitaxy *Appl. Phys. Lett.* **114** 103101
[62] Saket O, Bayle F, Himwas C, Piazza V, Patriarche G, Cattoni A, Collin S, Oehler F, Travers L, Julien F, Harmand J-C and Tchernycheva M 2020 Nanoscale electrical analyses of axial-junction GaAsP nanowires for solar cell applications Nanotechnology **31** 145708
[63] Van Treeck D, Fernández-Garrido S and Geelhaar L 2020 Influence of the source arrangement on shell growth around GaN nanowires in molecular beam epitaxy *Phys. Rev. Mater.* **4** 013404
[64] Tchoulfian P, Donatini F, Levy F, Dussaigne A, Ferret P and Pernot J 2014 Direct Imaging of p–n Junction in Core–Shell GaN Wires *Nano Lett.* **14** 3491–8